Available online at www.sciencedirect.com
ScienceDirect
European Journal of Mechanics B/Fluids 27 (2008) 591–608

On the breakup of bubbles at high Reynolds numbers and subcritical Weber numbers

Antonio Revuelta [a], Javier Rodríguez-Rodríguez [b], Carlos Martínez-Bazán [c,*]

[a] *División de Combustión y Gasificación, CIEMAT, 28040 Madrid, Spain*
[b] *Área de Mecánica de Fluidos, Universidad Carlos III de Madrid, Avda. de la Universidad 30, 28911 Leganés (Madrid), Spain*
[c] *Área de Mecánica de Fluidos, Universidad Jaén, Campus Las Lagunillas, 23071 Jaén, Spain*

Received 6 February 2007; received in revised form 11 October 2007; accepted 18 October 2007

Available online 7 November 2007

Abstract

In this paper we propose a simplified two-dimensional model to describe some aspects of the turbulent breakage of bubbles at subcritical Weber numbers. In particular we focus on the breakup of bubbles owing to their interaction with an array of successive eddies, modeled by a train of straining flows. Our simulations show that, under certain conditions, a bubble accumulates energy due to its interaction with a sequence of turbulent structures until it eventually breaks, even if none of the eddies is sufficiently energetic to split the particle by itself. It is also shown that the different strain directions of the eddies acting on the surface of the bubble, and the resonance effect between their characteristic frequency and the natural oscillation frequency of the bubble immersed into the straining flow are the two key factors in the bubble deformation, and subsequent breakup mechanism. Moreover, the breakup patterns obtained from our simulations seem to agree qualitatively well with the experimental observations.

PACS: 47.55.dd; 47.55.df

Keywords: Bubble breakup; Subcritical Weber number; Straining flow

1. Introduction

The atomization of a gas bubble in a homogeneous and isotropic turbulent flow has received a wide attention through the years since Kolmogorov [1] and Hinze [2] formulated the principles of the classical theory of the turbulent atomization of droplets. Kolmogorov theory states that a particle immersed in a homogeneous and isotropic turbulent flow, whose characteristic size lies within the inertial subrange of the energy spectrum, eventually breaks if the turbulent pressure fluctuations acting on its surface are strong enough to overcome the surface tension, confining stresses. The ratio between both forces is commonly known as the turbulent Weber number, We. Thus, according to Kolmogorov, the turbulent breakup of a particle will take place if a properly defined Weber number is larger than a critical value, $We > We_c$. Although the Weber number is a relevant parameter of the breakup problem since it measures

* Corresponding author.
E-mail addresses: a.revuelta@ciemat.es (A. Revuelta), javier.rodriguez@uc3m.es (J. Rodríguez-Rodríguez), cmbazan@ujaen.es (C. Martínez-Bazán).

0997-7546/$ – see front matter
doi:10.1016/j.euromechflu.2007.10.004

the amount of turbulent kinetic energy available at the bubble scale, the fact that a particle can also break for arbitrarily small values of *We* is widely accepted. For example, a situation where the sub-critical breakup of bubbles may occur is given when the initial deformation of the bubble is sufficiently large. However, a different scenario was experimentally described by Risso and Fabre [3], who identified a new breakup mechanism, denoted by the authors as *resonance mechanism*, occurring at Weber numbers around the critical one, $We \sim We_c$. In this situation, although a single eddy was not able to split the bubble, a succession of eddies could deform it progressively, leading to an accumulation of energy that eventually might cause its rupture. The authors indicated that this mechanism could successfully split a bubble if its residence time within the turbulent field was sufficiently long, provided that the damping rate that limits the energy that the bubble can accumulate during its fluctuating deformation is not larger than the arrival frequency of turbulent eddies. Finally, they also introduced the new concept of the *eddy efficiency* to take into account the dynamic response of the bubble to different patterns of eddies. Previously, Sevik and Park [4] also postulated a different type of resonance mechanism between the bubble dynamics and the turbulent fluctuations, and indicated that a bubble of radius a_0, immersed in a turbulent flow might split if its natural frequency, which corresponds to the second eigenmode (predominantly observed in the experiments), was of the order of the characteristic frequency of the turbulent fluctuations of eddies of characteristic size $l_e \sim a_0$.

Rodríguez-Rodríguez, Gordillo and Martínez-Bazán [5] showed that a model given by a gas bubble immersed in an uniaxial straining flow (USF), in the limit $Re \to \infty$, could describe some fundamental aspects of the bubble breakup process in a turbulent flow at $We > We_c$. Furthermore, they also showed that the breakup times obtained with their model agreed fairly well with the experimental results in real turbulent flows reported by Martínez-Bazán, Montañes and Lasheras [6]. Previously, Kang and Leal [7,8] studied the dynamics of bubbles in a straining flow and demonstrated that large deformations, promoted by small fluctuations of the flow strength of characteristic frequency close to the natural oscillation frequency of a bubble immersed in the flow, may take place at sub-critical Weber numbers [8]. However the efficiency of this mechanism is limited by the residence time of the bubble within the straining flow generated by such eddies [9].

Although Kang and Leal performed a comprehensive study of the effect of the main parameters of the problem, i.e. the Reynolds number, the Weber number and the frequency of the straining flow, they only considered flows with a fixed axis of strain. To improve those models it would be necessary to consider a flow whose main axis of deformation was allowed to vary randomly with time; a situation closer to what actually happens in real turbulent flows. Unfortunately, this feature cannot be implemented in an axisymmetric flow, and three-dimensional simulations would be necessary. Thus, the present work is intended to be an intermediate step between the axisymmetric models described above and the more realistic three-dimensional simulations that are still rare in the literature.

At this point, it should be mentioned the recent work by Qian et al. [10], who performed three dimensional numerical simulations of the bubble dynamics in a homogeneous turbulent flow using the Lattice Boltzmann method. Part of their results, as the stochastic character of the bubble breakup, agree with the experimental findings of Risso and Fabre. However, due to the high computational cost of the simulations, a very limited number of cases were reported and, consequently, this work does not present significant statistical results. In addition, other limitations, which may lead to discrepancies with experiments, are also pointed out in this investigation, i.e. the finite size of the computational domain, the associated interaction among bubbles, the sensitivity to initial conditions and the limited simulation time.

Similar to most of the turbulent particle breakup models found in the literature, in the present one we will assume the bubbles to be much larger than the Kolmogorov dissipation length scale. However, related to the complementary sub-Kolmogorov regime – that is particles smaller than the dissipation length scale – it is worth mentioning the work by Cristini et al. [11], who studied the deformation and breakup of droplets in an isotropic, turbulent flow using a pseudospectral representation of the turbulent outer flow, coupled to 3D-boundary integral simulations of the local drop dynamics.

One of the objectives of the present work is to shed some light on the different effects to be considered in order to formulate statistical models for the turbulent breakup of bubbles, and in particular for their breakup frequency. As it was shown in Lasheras et al. [12], simple phenomenological models based on kinematic considerations could predict the experimental data considerably well at large Weber numbers. However, the complexity of the breakup at lower Weber numbers does not allow the use of this type of simple models [3].

Although the present model is restricted to two dimensions, whose limitations are evident, we believe that it still captures some important physical aspects of the bubble breakup at low Weber numbers. Therefore, the results obtained

by the least expensive two-dimensional computations can help to understand the complex dynamics occurring in more realistic three-dimensional cases. On the other hand, two-dimensional approximations of the drop/bubble dynamics into a flow field that reveal interesting phenomena are quite usual in the literature. For example, it can be mentioned the work by Sarkar and Schowalter [13], whose two-dimensional computations of the drop dynamics at low Reynolds numbers in extensional flows displayed a resonance phenomena that was later on confirmed by their subsequent three dimensional simulations [14].

2. Model description

The flow field considered in this work, and illustrated in Fig. 1, consists of a bubble subjected to a pulsating uniaxial, straining flow (USF) whose strain direction, $\theta(t)$, varies randomly for every pulse. The pulse train is defined by two different times, $\tilde{T}_1$ and $\tilde{T}_2$ respectively. Here $\tilde{T}_1$ represents the duration of the straining flow, or in other words the time of the bubble-turbulent eddy interaction, whereas $\tilde{T}_2$ is the period of the pulse train. Thus, according to this definition, $\tilde{T}_2 - \tilde{T}_1$ simply indicates the time between two successive bubble-eddy interactions. The equations governing the dynamics of the bubble, written in dimensionless form, are:

$$\nabla \cdot \vec{v}_{(\mathrm{g,l})} = 0, \tag{2.1}$$

$$\partial_t \vec{v}_\mathrm{l} + (\vec{v}_\mathrm{l} \cdot \nabla)\vec{v}_\mathrm{l} = -\nabla p_\mathrm{l} + Re^{-1} \nabla \cdot \mathbf{D}_\mathrm{l}, \tag{2.2}$$

$$\partial_t \vec{v}_\mathrm{g} + (\vec{v}_\mathrm{g} \cdot \nabla)\vec{v}_\mathrm{g} = -(1/\rho_\mathrm{g})\nabla p_\mathrm{g} + (Re\rho_\mathrm{g}/\mu_\mathrm{g})^{-1} \nabla \cdot \mathbf{D}_\mathrm{g}, \tag{2.3}$$

where the subindexes (g, l) refer to magnitudes related to the gas and liquid phase respectively, and $\mathbf{D}_{(\mathrm{g,l})}$ is twice the rate of deformation tensor. To make the problem dimensionless, the liquid density, $\tilde{\rho}_\mathrm{l}$, the bubble radius, a_0, and the inverse of the maximum strain rate, $1/M_0$, were selected as the characteristic density, length and time respectively. The viscosity of the liquid phase, $\tilde{\mu}_\mathrm{l}$, was used to scale the viscosity of the gas phase, $\tilde{\mu}_\mathrm{g}$, thus $\rho_\mathrm{g} = \tilde{\rho}_\mathrm{g}/\tilde{\rho}_\mathrm{l}$ and $\mu_\mathrm{g} = \tilde{\mu}_\mathrm{g}/\tilde{\mu}_\mathrm{l}$ in Eq. (2.3). The above equations must be completed with the proper boundary conditions. For the liquid phase, the flow far away from the bubble should tend to the inviscid and irrotational flow derived from the following unsteady velocity potential,

$$\Phi(x, y, t) = M(t)\big(0.25(x^2 - y^2)\cos\theta + 0.5xy\sin\theta\big), \tag{2.4}$$

where $M(t) = \sum_{n=0}^{\infty}[\mathrm{H}(t - nT_2) - \mathrm{H}(t - nT_2 - T_1)]$, with H being the Heaviside function and $\theta(t)$, which will be randomly varied from pulse to pulse, the angle between the axis of strain and the x-axis. Moreover, T_1 and T_2 are the dimensionless strain pulse duration and repetition rate respectively. On the other hand, the pressure jump across the liquid–gas interface is given by the continuity of normal stresses,

$$Re^{-1}(\mathbf{D}_\mathrm{l} - \mu_g \mathbf{D}_\mathrm{g}) \cdot \vec{n} = (p_\mathrm{l} - p_\mathrm{g} + We^{-1}\nabla \cdot \vec{n})\vec{n}, \quad \text{and} \quad \vec{v}_\mathrm{l} = \vec{v}_\mathrm{g}. \tag{2.5}$$

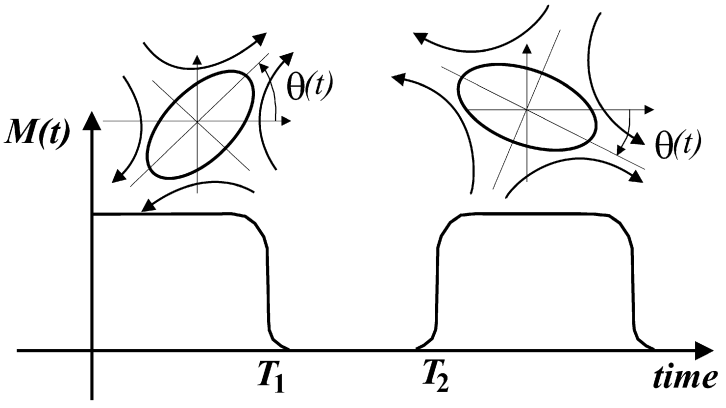

Fig. 1. Sketch of the two-dimensional model considered in the present work. The bubble is subjected to a train of pulses of straining flow separated by a period when the flow is turned off. The angle of the axis of the straining flow, θ, is randomly varied from pulse to pulse, although it is kept constant through the duration of the pulse.

As summary, with the present formulation the problem depends on the following set of dimensionless parameters: the gas-to-liquid density and viscosity ratios, ρ_g and μ_g respectively, the Reynolds number, $Re = \tilde{\rho}_l a_0^2 M_0/\tilde{\mu}_l$, the Weber number, $We = \tilde{\rho}_l a_0^3 M_0^2/\sigma$, where σ is the gas–liquid surface tension, the dimensionless period of the pulse train, T_2, and the dimensionless duration of the strain pulses, T_1.

To reduce the number of parameters of the problem, we will limit the study to the case of air bubbles in water, thus $\rho_g = 0.0012$ and $\mu_g = 0.018$ through all the simulations. Moreover, since we are interested in the dynamics of bubbles whose sizes lie within the inertial subrange of the turbulent energy spectrum, the local Reynolds number is expected to be large. Therefore, in our study the Reynolds number will be kept constant and equal to $Re = 500$, a value sufficiently large to consider the viscous effects nearly negligible in the breakup process [9].

An additional simplification is that our study will be restricted to values of the pulse duration time, T_1, of order unity. This assumption is consistent with the fact that we are interested in describing the interaction of a bubble with turbulent structures of roughly its same size, which are the ones that more efficiently lead to the bubble breakup [1,15]. Assuming that the bubble is immersed into an isotropic and homogeneous turbulent flow, at a given time, the velocity difference between two points a distance a_0 apart is of the order $\Delta u \sim \varepsilon^{1/3} a_0^{1/3}$, with ε being the dissipation rate of turbulent kinetic energy per unit mass and per unit time. At the same time, the maximum velocity difference that the straining flow produces along the perimeter of the bubble is of the order $M_0 a_0$. Thus, to model the effect of the turbulent structures of interest on the bubble, the flow intensity should be of the order $M_0 \sim \varepsilon^{1/3} a_0^{-2/3}$. On the other hand, notice that $\tilde{T}_1$ can be understood as the lifetime of the turbulent structure, which is of the order $\tilde{T}_1 \sim a_0^{2/3} \varepsilon^{-1/3}$ or, similarly, the inverse of the strain rate. However, it must be pointed out that, although dimensional arguments allow us to predict the order of magnitude of the pulse duration, its precise value is undetermined by a constant of order unity. Note that the above discussion would still be valid in the case of two dimensional turbulence, since both the velocity difference between two points, Δu, and the lifetime of a turbulent eddy, $\tilde{T}_1$, follow the same scaling laws with a_0 and ε.

Finally, the velocity boundary conditions defined in our model involve a qualitative behavior similar to that of the droplet dynamics described by Cristini et al. [11], with successive elongations and relaxations of the particle before the breakup event. The consequent bubble dynamics is also consistent with the experimental observations of bubbles in turbulent flows, where it can be observed that bubbles oscillate during most of the time with moderately low amplitudes, which sometimes increase suddenly. However, it must be indicated that the purpose of the present approach is simply to describe the interaction of the bubble with singular turbulent structures rather than with the continuous distribution of eddies that would exist in a real turbulent flow. Thus, the influence of the turbulent flow on the local dynamics of the bubble is determined a priori through the far-field velocity boundary conditions, and only the strain direction is stochastic, to allow us to describe the effect of T_1, T_2 and We on the bubble breakup.

3. Numerical scheme

The incompressible, dimensionless, two-phase flow Navier–Stokes equations (2.2)–(2.3) were solved using the level-sets method [16,17]. The local density and viscosity were determined by the value of the level-set function ϕ, which is simply a measure of the distance to the interface, and whose evolution is given by the advection equation

$$\partial_t \phi + \vec{v}_l \cdot \nabla \phi = 0, \tag{3.1}$$

with the zero level-set $\phi = 0$ indicating the bubble interface.

The Navier–Stokes equations were integrated in a staggered grid, using a implicit temporal scheme, with a Crank–Nicholson scheme for the viscous terms, and an Adams–Bashforth one for the convective terms, which were spatially discretized with third-order ENO schemes. The variable density projection method used, by which the velocity field at the end of every temporal step is made divergence-free, requires the solution of a pseudo-Poisson equation of the form $\nabla \cdot (\rho^{-1} \nabla \phi) = \nabla \cdot u^*$ for the pressure increment field ϕ, where u^* is the intermediate velocity field. This Poisson equation was discretized by a second-order scheme and the corresponding linear system was solved by a robust, unsymmetric, multifrontal method (UMFPACK) especially designed to solve sparse linear systems [18]. It is worth to remark that this Poisson solver and the use of the ENO schemes for the convective terms constitute fundamental elements to accurately solve cases with severe deformations, low Weber numbers and the density and viscosity ratios considered, that could not be solved using centered schemes and standard iterative Poisson solvers.

The level-set equation was integrated in a narrow band, in the neighborhood of the interface, with a semi-implicit second-order advection operator partition. The initial condition used for the simulations corresponded to a flow field initially at rest, with a spherical bubble placed at the stagnation point of the imposed unsteady hyperbolic field. In addition, the strain steps were slightly smoothed to avoid the effect of a sudden change in the boundary conditions which would cause strong pressure pulses and might lead to unrealistic bubble breakups.

Furthermore, when the function ϕ is integrated in time, it can be affected by the numerical diffusion of the code and distorted by the flow field. Thus, to keep ϕ as a function that measures the distance from the interface, a new distance function was included every time step, solving the so-called re-distance equation [17]. This equation was solved with a RK3 temporal scheme and third-order ENO schemes for the convective terms.

The present numerical code constitutes a two-dimensional version of our previous axisymmetric one used in Revuelta et al. [9], which was validated with the examples presented in Sussman and Smereka [16]. In that work, we showed that the level-set method is able to accurately determine the critical Weber number We_c and the breakup times t_b if the grid employed is fine enough. The adequate grid resolution was determined comparing the breakup times obtained at high Reynolds numbers with the results given by a boundary element code (limit $Re \to \infty$). Thus, in the present investigation a resolution similar to that of Revuelta et al. [9] was used, with an interfacial thickness parameter, ϵ, equal to $\epsilon = 1.5\Delta$, where Δ represents the grid spacing. Our numerical tests showed that the value of the critical Weber number We_c, was not significantly affected by the grid resolution for the flow fields type considered here. In fact, we obtained a critical Weber number of $We^{2D}_{crit} = 1.80 \pm 0.01$ for the steady USF using grid spacings $\Delta = 0.033$ and $\Delta = 0.050$ respectively, and of $We^{2D}_{crit} = 1.82 \pm 0.01$ using a coarser grid size, $\Delta = 0.067$. The value of the critical Weber number was determined running different simulations where the Weber number was varied in steps of $\Delta We = 0.01$ until the bubble breakup was observed. The main difference encountered with the different grid resolutions was the presence of more and larger satellites bubbles after the breakup event when the resolution was not sufficiently fine as shown in Fig. 2. The figure shows that, for sufficiently fine grid spacing, the breakup time is nearly unaffected by the grid resolution although the size of the satellite bubbles increases with Δ. Furthermore, it should be remarked that although the numerical method may not properly describe the final stages of the bubble breakup process, it does not significantly affect the values of the critical Weber number and the breakup time since the final collapse of the neck of the bubble occurs at times very short compared with the characteristic time of the prob-

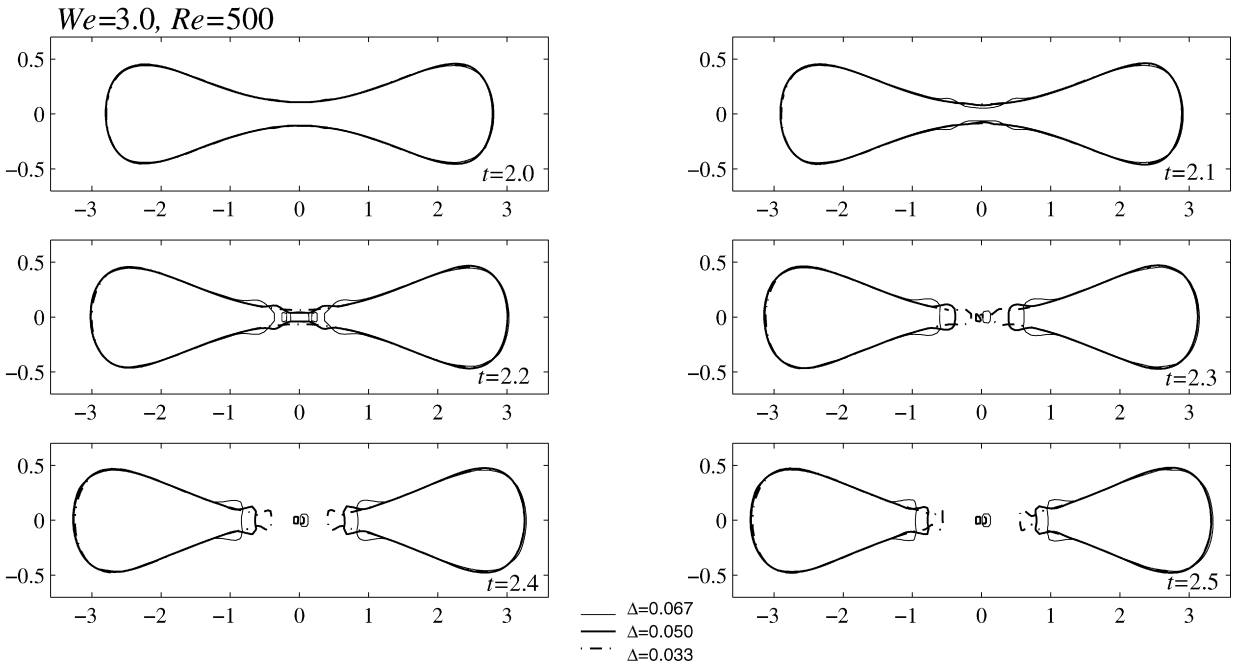

Fig. 2. Comparison of the results obtained in a test case for different values of the grid resolution. Notice that although the size of the satellite bubble increases with the grid spacing, the break up time remains nearly unaffected.

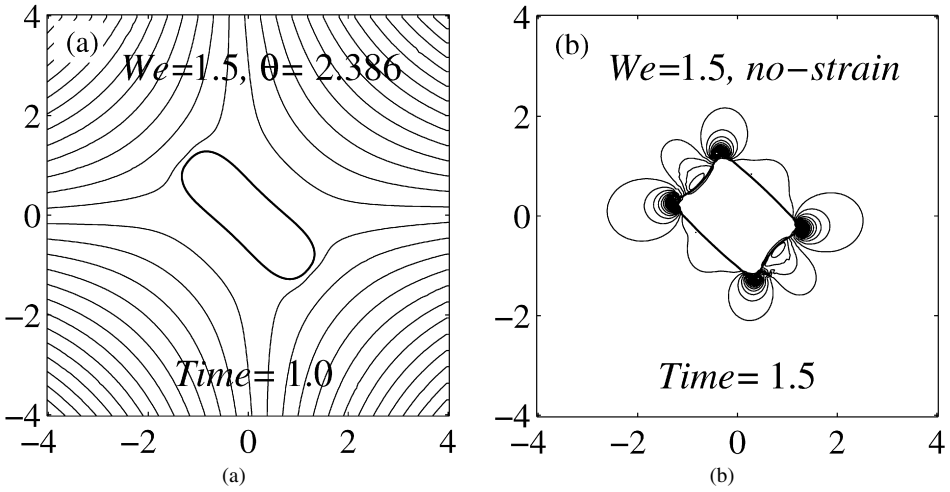

Fig. 3. Pressure contours at $We = 1.5$ and two different times of the uniaxial straining flow considered: (a) strain pulse with $\theta = 2.386$ and (b) no-strain interval. The pressure difference between isolines is $\Delta p = 3$ in Fig. 3(a) and $\Delta p = 0.3$ in Fig. 3(b).

lem investigated herein, as it was shown by Gordillo et al. [19]. The results presented below correspond to a domain $(x, y) = [-4, 4] \times [-4, 4]$ and a uniform grid NX × NY = 160 × 160, for which it was proven that mass losses were always below 0.5% before the breakup instant.This grid resolution included 1260 grid points into the initial circular bubble.

As example of the numerical results obtained, two different pressure contours are shown in Fig. 3 for $We = 1.5$ and two different instants of the simulation. Fig. 3(a) corresponds to a strain pulse while Fig. 3(b) corresponds to an instant with no-strain. The pressure difference between isolines is $\Delta p = 3$ in Fig. 3(a) and $\Delta p = 0.3$ in Fig. 3(b).

4. Results

4.1. Bubble dynamics in a steady Uniaxial Straining Flow

Similar to the axisymmetric case, well-reported in the literature (see Kang and Leal 1987 [7] and Kang and Leal 1990 [8] and references therein), our numerical simulations revealed that a two-dimensional bubble immersed into a steady USF breaks if its corresponding Weber number is larger than a critical value. Thus, the integration of the bubble evolution in the steady, bidimensional, uniaxial straining flow provided with a reference critical Weber number of $We_c^{2D} \approx 1.80$. Note that the critical Weber number obtained in the two-dimensional, straining flow studied here slightly differs from the value reported by Revuelta et al. [9] in an axisymmetric flow, $We_c = 2.225$. It should also be mentioned that We_c does not depend on Re for values of Re sufficiently large [9].

At supercritical Weber numbers, two significant results obtained from the simulations are the breakup time as well as the breakup deformation, or interfacial length, at the breakup instant (interface surface in the three-dimensional counterpart). The relevance of the breakup time in determining the functional relationship between the experimentally observed breakup frequencies and the Weber number was discussed in Rodríguez-Rodríguez et al. [5] for the axisymmetric case. As in that case, the breakup time decreases with increasing Weber number, approaching the characteristic convective time, $t = 1$, in dimensionless formulation, when We tends to infinity. The values of the interface length at the instant of breakup constitute a reference value for the simulations in the unsteady USF presented in the following subsection. Some values of the ratio between the interface length at the breakup instant, S, and the initial one, $S_0 = 2\pi$, for different Weber numbers are $S/(2\pi)(We) = 1.82(1.85), 1.85(2.0), 2.1(3.0), 1.89(5.0), 1.76(10), 1.68(50)$.

On the other hand, at subcritical Weber numbers, the bubble oscillates into the USF with a frequency that increases as We decreases. Fig. 4(a) shows the oscillation of the bubble length along the x-axis, D, for different subcritical Weber numbers. As already mentioned in Revuelta et al. [9] for the axisymmetric case, the bubble tends to escape from the USF stagnation point at times of the order O(10). This fact prevents an accurate calculation of the oscillation frequency for the different Weber numbers. Moreover, in the unsteady case with a constant axis of strain, this effect also avoids

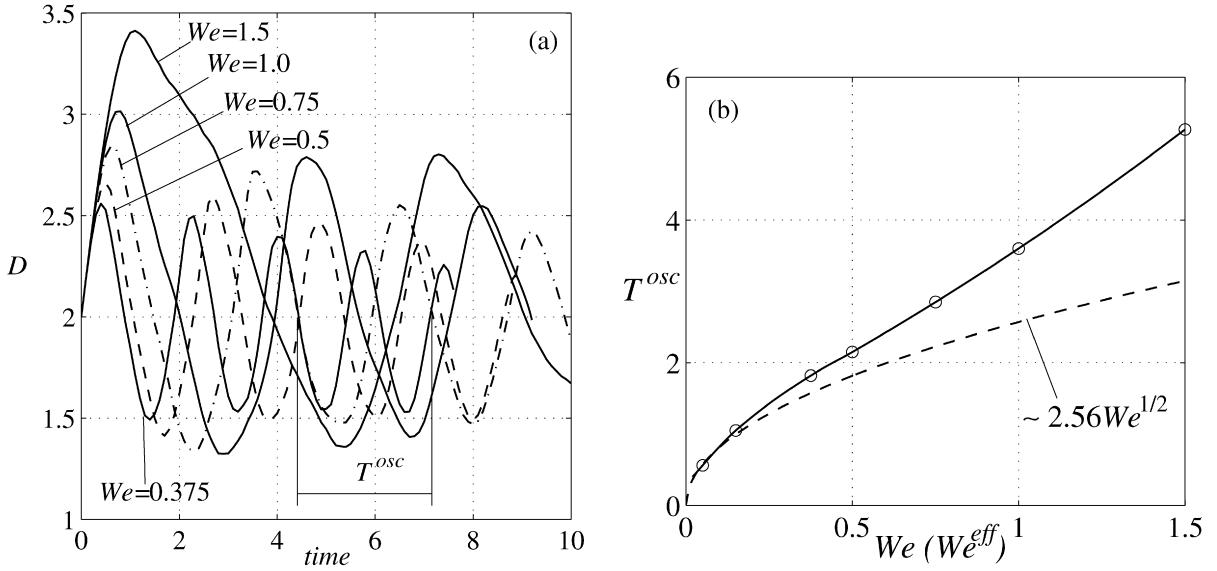

(a) (b)

Fig. 4. (a) Oscillations of the bubble length along the x-axis, D, of a bubble inside a steady USF, for different subcritical Weber number. (b) Dependence of the oscillation period on the Weber number. The dashed line corresponds to the solution yielded by the asymptotic description at $We \ll 1$ given in Appendix A, with $T_2^{\mathrm{osc}} = 2\pi/\omega_2 = \sqrt{2/3}\,\pi\, We^{1/2}$.

the bubble breakage due the resonance mechanism proposed by Kang and Leal [8], where small fluctuations of the USF strength at the natural oscillation frequency of the bubble causes large deformations, leading to the bubble breakup at very long times. However, the limited residence time of the bubble in the USF makes necessary larger fluctuations of order O(1) to break the bubble. Approximate values of the oscillation periods at subcritical Weber numbers are $T^{\mathrm{osc}}(We) = 1.85(0.375), 2.15(0.5), 2.85(0.75), 3.60(1.0), 5.27(1.5)$. Furthermore, Fig. 4(b) shows the dependence of the bubble oscillation period with the Weber number, together with the asymptotic behavior when $We \ll 1$ given by $T_n^{\mathrm{osc}} = 2\pi/\omega_n \sim We^{1/2}$ (dashed line) and described in Appendix A.

4.2. Bubble dynamics in the unsteady Uniaxial Straining Flow

Since in a pulsating straining flow the intensity of the outer flow, $M(t)$, varies with time, the deforming stresses acting on the surface of the bubble also change with time, and an alternative effective Weber number based on the time average strain intensity over one period should be defined. Thus, since the Weber number can be understood as the squared ratio between the capillary time, $(\tilde{\rho}_1 a_0^3/\sigma)^{1/2}$, and the convective time, $1/M_0$, the effective Weber number should be defined using the squared time ratio $(T_1/T_2)^2$ as the averaging factor, giving

$$We^{\mathrm{eff}} = We\left(\frac{T_1}{T_2}\right)^2. \tag{4.1}$$

It will be shown later on in this section that there is a resonance mechanism between the frequency of the strain pulses and the oscillation frequency of the bubble into the steady USF corresponding to the averaged or effective Weber number, We^{eff}.

The temporal oscillations of the length of the bubble interface, S, have been shown in Fig. 5 for some representative cases with the aim at quantifying the evolution of the bubble deformation. In this figure, the crosses indicate the breakup instant. As expected, the total interfacial length of the bubble increases with time until the bubble breaks. Notice that S is not just a measure of the bubble deformation but also a measure of the surface energy that the bubble accumulates during its interaction with a sequence of strain pulses. This deformation process is similar to the accumulation of energy due to the bubble interaction with a sequence of eddies in a turbulent flow described by Risso and Fabre [3]. More importantly, a detailed observation of Figs. 5(a) and 5(b), corresponding to subcritical Weber numbers, $We = 1.0, 1.5$, reveals that the subcritical breakup usually occurs at a given level of deformation or,

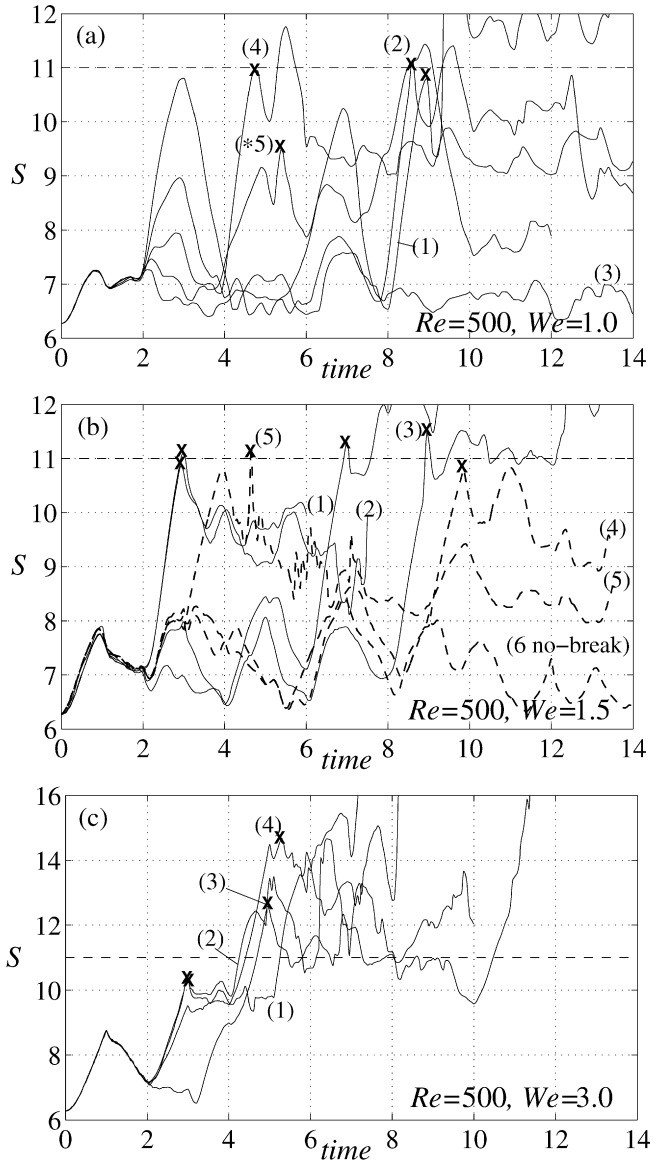

Fig. 5. Temporal evolution of the bubble interfacial length, S, at $Re = 500$, (a) $We = 1.0$, (b) $We = 1.5$ and (c) $We = 3.0$. $T_1 = 1$, $T_2 = 2$ unless otherwise indicated. Dashed lines in Fig. 5(b) correspond to situations where $T_2 = 3$.

similarly, surface energy, $S/(2\pi) \approx 1.75 (S \approx 11)$. This point is clearly observed in Fig. 6 which displays the relative frequencies of occurrence of the different values of S at the breakup instant. Notice that, although the mean value of the distributions are nearly the same, $S_m/(2\pi) \approx 1.75$, they become narrower as the Weber number decreases. This result suggests that for low enough Weber numbers, the relevant parameter that determines whether the bubble breaks or not at a given time is the instantaneous surface energy, independently of the intensity of the outer flow or the detailed history of the deformation process. In other words, the bubble accumulates surface energy during the deformation process until eventually breaks when S reaches a certain value.

This observation is consistent with the results provided by the linear analysis of the small amplitude oscillations of the bubble at $We \ll 1$, and described in Appendix A. In fact, Eq. (A.16) shows that, at first order, the outer flow is only able to transfer energy to the second eigenmode, corresponding to the eigenfunctions $(\cos 2\alpha, \sin 2\alpha)$. These eigenfunctions are precisely associated with deformations qualitatively equal to the ones observed in most of the cases (dumbbell-shaped bubbles). The transfer of energy to other modes only occurs due to higher order effects which

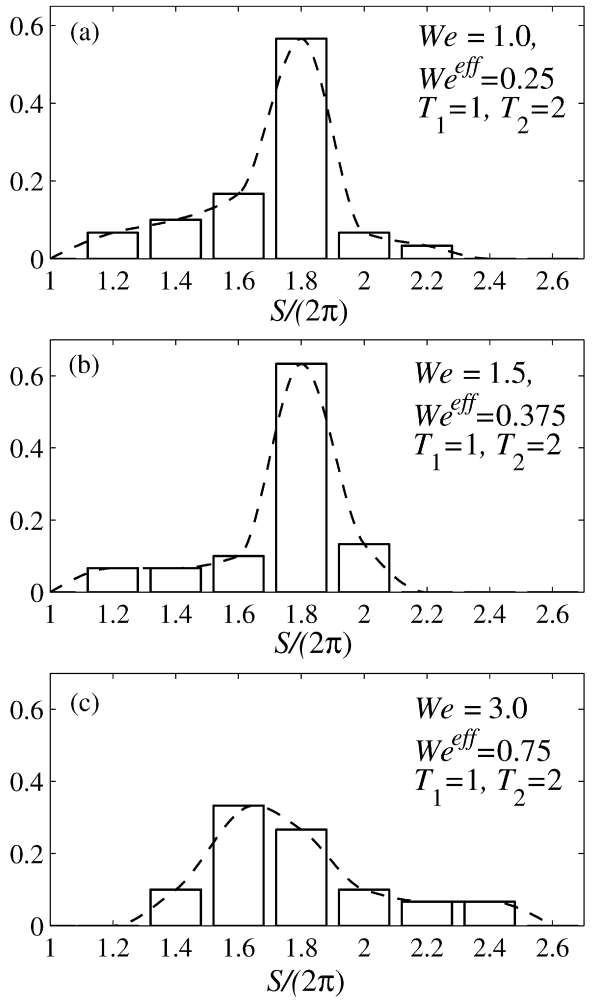

Fig. 6. Relative frequency of the values of the bubble deformation, $S/(2\pi)$, at the breakup instant for three sets of simulations corresponding to different Weber numbers: (a) $We = 1.0$, (b) $We = 1.5$ and (c) $We = 3.0$. Here $T_1 = 1, T_2 = 2$.

are sufficiently slow to be appreciated in most of the simulations. Interestingly, Risso and Fabre [3] reported similar observations for air bubbles immersed in a turbulent flow; the oscillations described by the bubbles, although chaotic, projected onto the second eigenmode with much larger amplitudes than on higher order modes.

Fig. 7 shows the influence of the period of the strain pulses train, T_2, on the value of the breakup deformation. In this case of $T_1 = 1$, changes of T_2 are equivalent to changes in the intermittency of the modeled turbulent flow. When the frequency of the eddies train is similar to the oscillation frequency of the bubble immersed in a steady USF whose Weber number is equal to the effective Weber number of the pulsating USF, We^{eff}, there is a maximum in the histogram, at approximately $S/(2\pi) = 1.7$–1.9, that corresponds to binary breakups, as can be observed in Fig. 7(b). Breakup events occurring at higher values of $S/(2\pi)$ correspond to smaller fragments separating from an irregular shaped mother bubble. Furthermore, when the frequency of the train is higher than the bubble oscillation frequency, (Fig. 7(a)), the maximum of the distribution moves to lower deformation values, although most of the breakup events are still binary. However, in this case, elongated bubbles which break in three or more fragments of approximately the same size are also observed, corresponding to the events of larger values of $S/(2\pi)$ in this histogram. Finally, when the train frequency is lower than the oscillation one, (Fig. 7(c)), the maximum of the histogram also translates to lower values of $S/(2\pi)$, but with only a few binary breakup events, and with a mother bubble forming one or two small daughter bubbles and a larger one in most of the events. It must be said that, in this case, a high percentage ($\sim 25\%$) of the simulations did not show any breakup event, with a maximum simulation time of $T_{\max} = 15$.

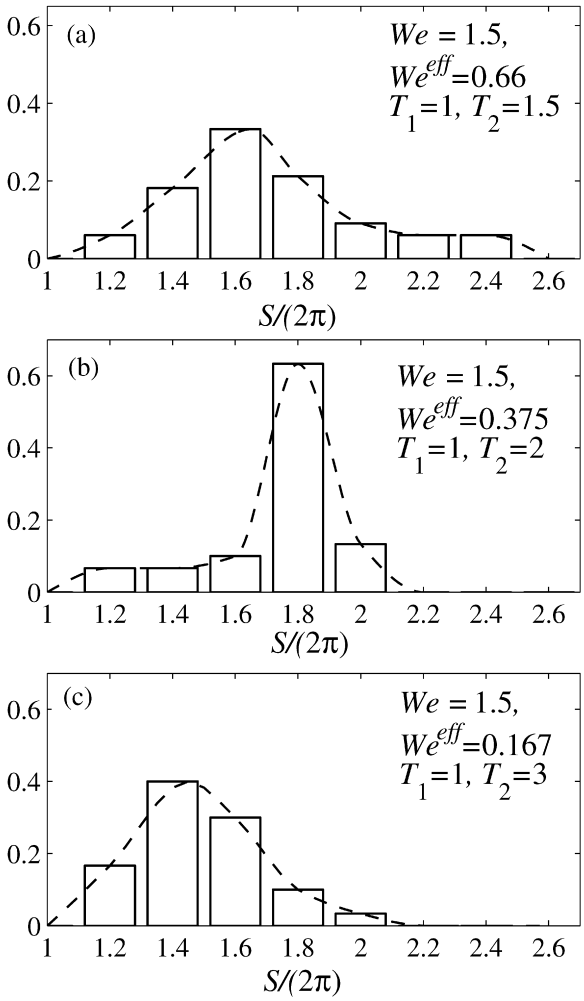

Fig. 7. Relative frequency of the values of the bubble deformation, $S/(2\pi)$, at the breakup instant for three sets of simulations corresponding to Weber number $We = 1.5$, $T_1 = 1$ and different values of the period of the straining flow: (a) $T_2 = 1.5$, (b) $T_2 = 2$ and (c) $T_2 = 3$.

Moreover, we also performed simulations for decreasing values of the eddy-bubble interaction time, T_1, which revealed that there is a minimum value of T_1 necessary for the bubble to split. For example, our simulations did not display any breakup event at $We = 1.5$ when $T_1 = 0.5$ and $T_2 - T_1 \neq T_1$, with a maximum simulation time of $T_{\max} = 15$. However, for $We = 1.5$, only in the cases with $T_1 = 0.5$ and $T_2 = 1$, a few breakup events, consisting of one or two small fragments separating from a bulgy shaped bubble, were observed.

Fig. 8 displays the histograms of the breakup times for three representative cases: (a) $We = 1.5$, $T_1 = 1$, $T_2 = 1.5$, (b) $We = 1.5$, $T_1 = 1$, $T_2 = 2$ and (c) $We = 3.0$, $T_1 = 1$, $T_2 = 2$. Fig. 8(a) shows a bimodal distribution, with the breakup time ranging from $t_b = 3$ to 8.5, which indicates that in most of the cases it is necessary at least three strain cycles to break a bubble. In this figure the period of the straining flow, T_2, is smaller than the oscillation period of a bubble in the steady USF at the corresponding We^{eff}. The distribution of the breakup time depicted in Fig. 8(b) shows that, although the breakup time goes from $t_b = 2.5$ to 10, most of the breakup events occur within the second and third strain pulses, associated to the two maxima of the histogram in $t_b = 2.5 - 3.0$ and $t_b = 4.5 - 5.0$, which correspond to the final stage of the second strain pulse. This is a consequence of the resonance phenomenon between the period of the straining flow and the oscillation of the bubble in the averaged USF given by We^{eff}. Furthermore, notice that the resonance mechanism increases the bubble breakup rate with respect to the case shown in Fig. 8(a). The last case displayed in Fig. 8(c) corresponds to a supercritical Weber number. As in Fig. 8(a), the distribution is bimodal, but with the two maxima at $t_b = 3.0 - 3.5$ and $t_b = 5.0 - 5.5$, which correspond to the end of second and third strain

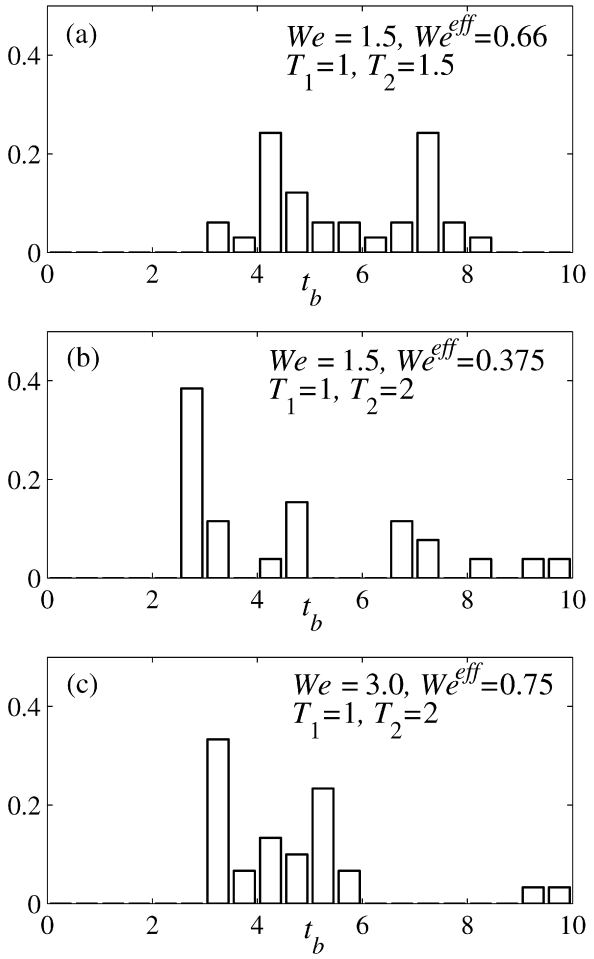

Fig. 8. Histograms of the breakup times corresponding to three representative cases: (a) $We = 1.5$, $T_1 = 1$, $T_2 = 1.5$, (b) $We = 1.5$, $T_1 = 1$, $T_2 = 2$, and (c) $We = 3.0$, $T_1 = 1$, $T_2 = 2$.

pulses respectively. Although in this case there is not resonance mechanism the breakup efficiency is similar to that of Fig. 8(b) simply because the Weber number is supercritical.

Furthermore, Fig. 9 shows the temporal evolution of the exchange of energy between the bubble and the outer, liquid flow, given by

$$E(t) = E_0 + \int_0^t \left[-\int_\Sigma p(\vec{v}\cdot\vec{n})\,\mathrm{d}\Sigma \right] \mathrm{d}t, \tag{4.2}$$

where $E_0 = (2\pi a_0\sigma)/(\tilde{\rho}_l \pi a_0^4 M_0^2) = 2/We$ is the initial surface energy of the undeformed bubble. In the steady, straining flow at subcritical Weber numbers, the energy transferred from the outer flow to the bubble increases from the initial, minimum value corresponding to the spherical bubble at rest, until it reaches a maximum. Once the maximum energy is achieved, it oscillates around an average value with a time decreasing amplitude due to the viscous damping, until the bubble runs away from the stagnation point at times $t \sim \mathrm{O}(10)$. However, in the unsteady cases the bubbles deform with time, accumulating surface energy until they eventually break when the deformation is sufficiently large. Moreover, our simulations indicated that the mean time required to break a bubble increases as the Weber number decreases, and that the averaged level of energy at the breakup time, t_b, was $E(t_b)/E_0 \approx 2.5$ as shown in Fig. 9. In addition, Fig. 10, which represents a characteristic example of the temporal evolution of the bubble deformation, $S(t)/(2\pi)$, and the energy extracted from the surrounding flow, $E(t)/E_0$, illustrates the relation between both magni-

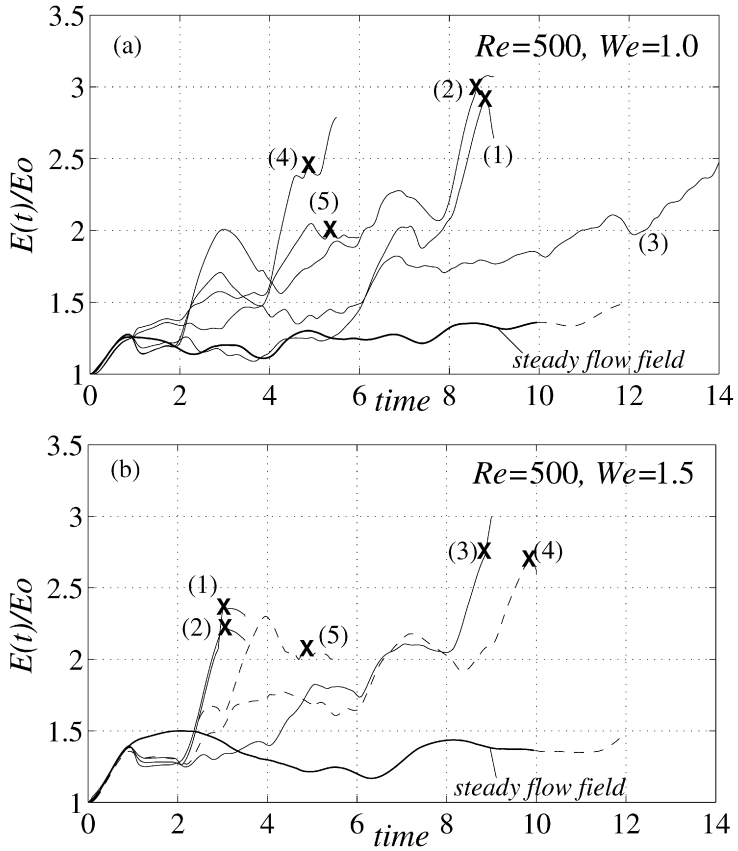

Fig. 9. Temporal evolution of the energy transferred from the outer flow to the bubble at $Re = 500$. (a) $We = 1.0$ and (b) $We = 1.5$. $T_1 = 1$, $T_2 = 2$ unless otherwise indicated. Dashed lines in Fig. 9(b) correspond to situations where $T_2 = 3$.

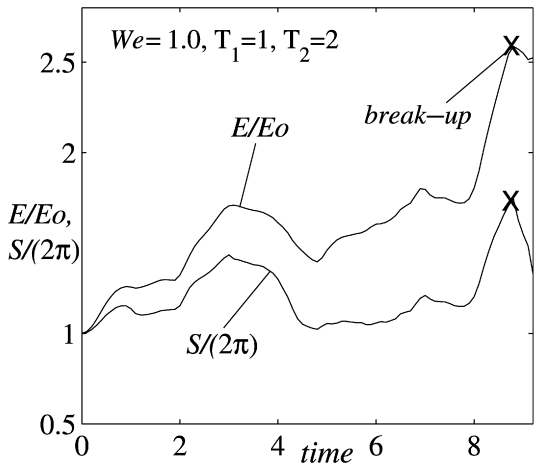

Fig. 10. Time evolution of the surface energy, $S/(2\pi)$, together with the energy exchanged with the outer flow, E/E_0, at $Re = 500$ and $We = 1.0$. Here $T_1 = 1$, $T_2 = 2$.

tudes. It is worth noticing that the energy extracted from the outer flow is always larger than the energy accumulated at the bubble interface, indicating that some energy is loss due to viscous dissipation. The difference between both curves is thus a measure of the energy dissipated due to viscous effects. Obviously, in the case of an inviscid fluid, both curves would collapse.

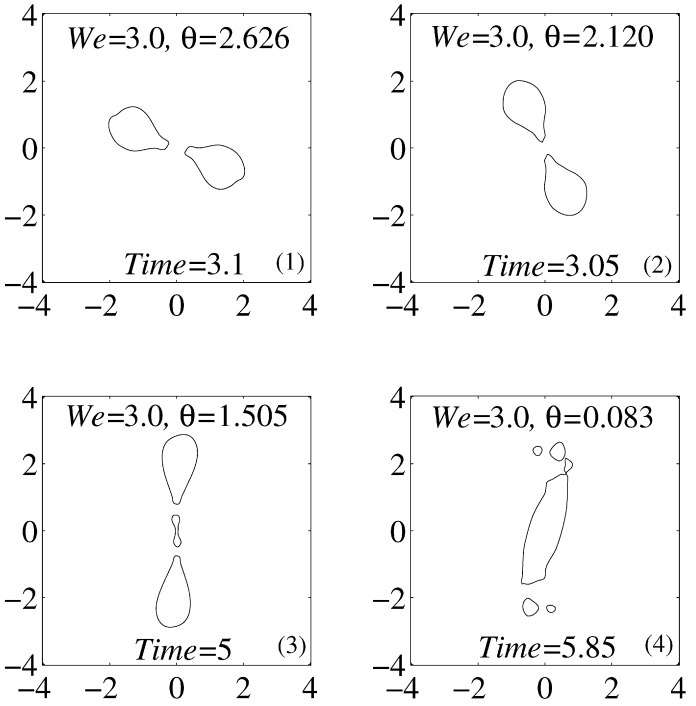

Fig. 11. Characteristic breakup patterns occurring at $We = 3.0$, $Re = 500$, $T_2 = 2$. The different patterns correspond to cases (1), (2), (3) and (4) shown in Fig. 5(c).

Regarding the different bubble breakup patterns, it was shown that the breakup events occurring at values of the surface deformation around $S/(2\pi) \approx 1.75 (S \approx 11)$, always corresponded to binary breakages. However we also observed that those breakups occurring at higher values of S generated multiple fragments of different sizes, associated to more diverse breakup patterns which commonly take place at higher values of the Weber number. This observation can be corroborated in cases (3) and (4) of Fig. 5(c). Moreover, Fig. 11 shows the breakup patterns generated in four of the simulations performed at a supercritical Weber number, $We = 3.0$, which correspond to cases (1), (2), (3) and (4) displayed in Fig. 5(c). Note that cases (3) and (4), whose breakup level of deformation is considerably larger than $S/(2\pi) \approx 1.75$, generated several daughter bubbles of different size. On the contrary, at subcritical Weber numbers all breakup patterns displayed similar characteristics: initially the bubble adopts a cigar shape before taking the form of a dumbbell, and finally breaks into two fragments of approximately the same size.

A relevant result that demonstrates the importance of the above mentioned eddy efficiency in the subcritical breakup process of bubbles is illustrated in Figs. 12 and 13. These figures show that bubbles break more easily in situations where the strain direction differs substantially from that of the previous cycle. In fact, when two consecutive strain directions are nearly perpendicular, $\Delta\theta \sim 90°$, the bubble suddenly increases its level of deformation breaking up at values of $S/(2\pi) \approx 1.75$ (Fig. 12). However, the breakup event does not usually take place when two consecutive strain directions are nearly parallel, $\Delta\theta \sim 0°$, (Fig. 13). This observation suggests the introduction of a new variable into the random eddy efficiency model proposed by Risso and Fabre, namely the difference of angle between two consecutive strain directions, $\Delta\theta$, or in other words, the difference between the strain direction and the direction of maximum deformation of the bubble. Thus, we can conclude that the energy that an eddy is able to transfer to the bubble depends not only on its intensity, but also on the entire history of turbulence and bubble deformation. To summarize this effect, Fig. 14 shows the temporal evolution of the interface length of a bubble subjected to two consecutive USF pulses whose strain directions have been varied from $\Delta\theta = 0°$ to $\Delta\theta = 90°$ in 10° steps. Notice that, in this case of $We = 1.5$, no breakup event occurred until $\Delta\theta > 50°$. Obviously the breakup efficiency of the *spatial succession of eddies* reported here increases with the Weber number and, for the same values of T_1 and T_2, the angle between two consecutive strain directions needed to break the bubble decreases as *We* increases. However, the pulse train and the bubble dynamics could interact in a more complex manner. Depending on the values of T_1 and T_2, if the

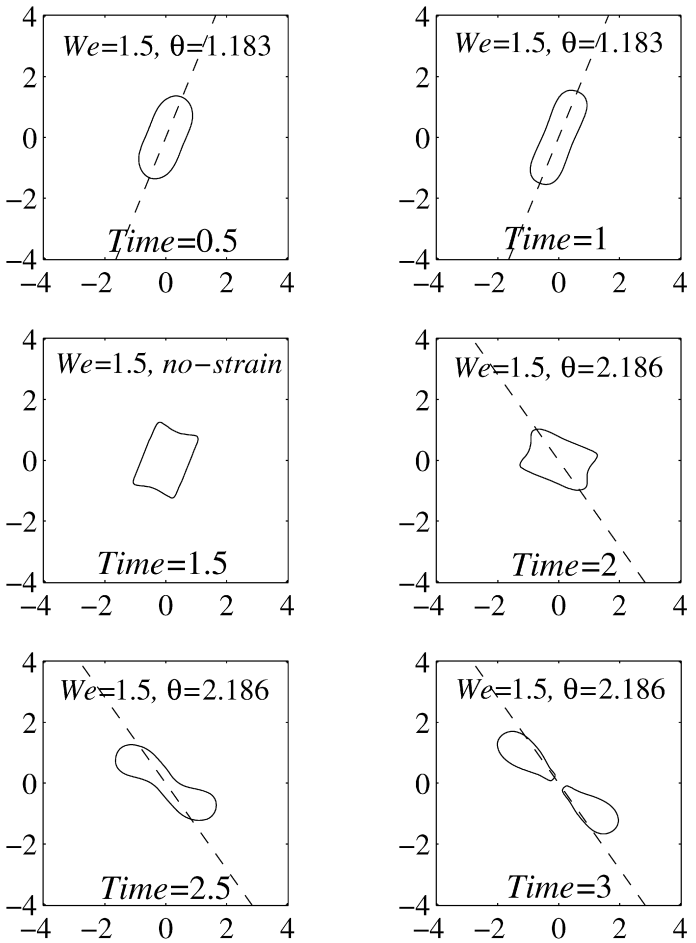

Fig. 12. Temporal evolution of the bubble interface until it breaks at $Re = 500$, $We = 1.5$, $T_2 = 2$. The sequence corresponds to case (1) of Fig. 5(b).

arrival of the strain pulse were in phase with the bubble oscillation, the bubble deformation would increase, otherwise it might decrease, as illustrated in description of the turbulent eddy-bubble dynamics interaction given by Risso and Fabre [3].

5. Discussion and conclusions

The dynamics of a two-dimensional bubble immersed in an unsteady flow consisting of a succession of randomly oriented straining flows has been studied. This simple flow may be useful to describe some aspects of the turbulent breakup of bubbles at subcritical Weber numbers. Thus, the model presented establishes a link between the classical USF model, and the experimental and theoretical description of the turbulent bubble breakup given by Risso and Fabre [3]. A first and interesting prediction of the model is that, regardless of its previous history, a bubble immersed in an unsteady flow at subcritical Weber numbers will most likely break at a given time if its surface energy (interface length in 2D), S, approximately reaches a certain value, given by $S/(2\pi) \approx 1.75 (S \approx 11)$ in our configuration. Such value is nearly the same as the breakup surface energy of bubbles in a steady USF whose Weber numbers are slightly larger than the critical one. Therefore, the surface energy emerges as a relevant parameter to control the stability of the bubble. The proposed explanation for this is that the energy is transferred primarily to the second vibration mode, $n = 2$, almost independently of the deformation history of the bubble; a result obtained assuming that the oscillations of the bubble can be described, at least qualitatively, by the linear dynamics valid for $We \ll 1$. In other words, the bubbles break mostly when the amplitude projected onto the second eigenmode, $n = 2$, reaches a critical

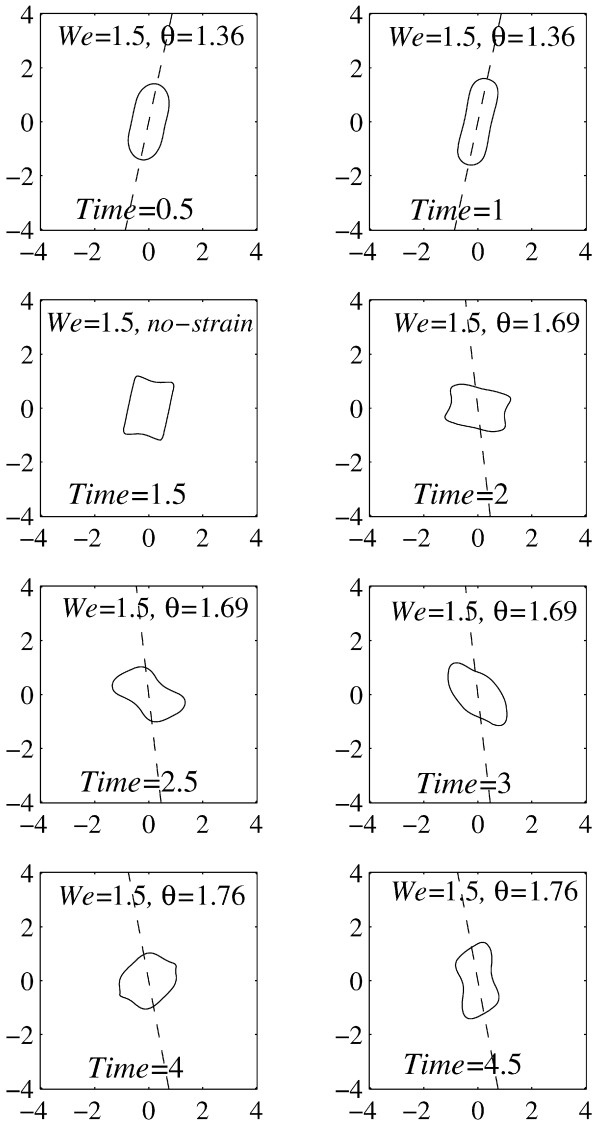

Fig. 13. Temporal evolution of the bubble interface until it breaks under the same conditions as those given in Fig. 12 but different sequences of strain directions. The evolution corresponds to case (3) of Fig. 5(b).

value. However, this explanation should be understood in a statistical way, meaning that the deformation histories in which the energy is transferred equally to multiple modes are possible, though not very often.

The observed existence of a given value S for which most of the breakups occur can be extended to the more realistic three-dimensional situation. In fact, axisymmetric simulations yielded a breakup surface energy for subcritical Weber numbers of $\tilde{S}/(4\pi a_0^2) \approx 1.37$. This value was obtained calculating the surface energy at the breakup instant of bubbles immersed in the corresponding steady flow, whose Weber numbers, $We = 2.25$ at $Re = 500$, are slightly larger than the critical one, $We_c(Re \gg 1) = 3.38\tilde{\rho}_l \varepsilon^{2/3} a_0^{5/3}/\sigma \approx 2.23$ [5,9]. It is worth mentioning that our critical Weber number agrees with the experimental value provided by Risso and Fabre [3] as $We = 2.0\tilde{\rho}_l \varepsilon^{2/3}(2a_0)^{5/3}/\sigma \approx 4.5$, who also postulated the idea of a minimum value of deformation, beyond which breakup events were observed for '*slight*' supercritical Weber numbers (see Fig. 6 in Risso and Fabre [3]).

Our simulations also showed that the increase in surface energy that the bubble experiences is closely related to the work that the outer fluid exerts on it. In addition, the model provides with a physical interpretation for the so-called *eddy efficiency*, understood as a measure of the amount of energy that a turbulent structure is indeed able to transfer

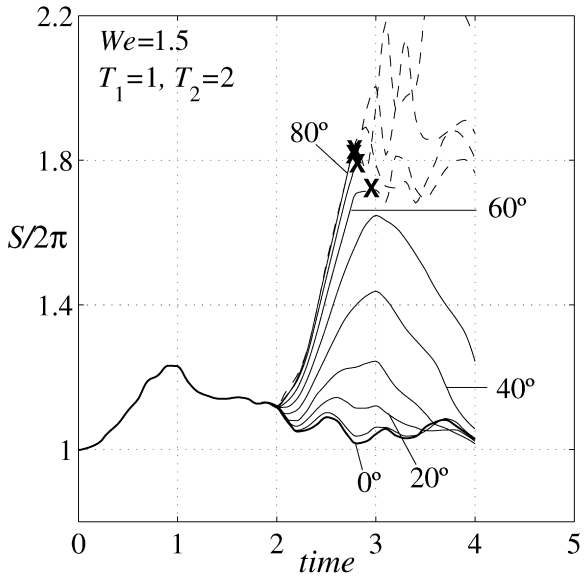

Fig. 14. Temporal evolution of the bubble interfacial length, $S/(2\pi)$ along two pulses whose strain directions differ an angle $\Delta\theta$ which has been varied from $\Delta\theta = 0°$ to $\Delta\theta = 90°$. Here $We = 1.5$ and $T_1 = 1$, $T_2 = 2$.

to the bubble. Additionally, the computations determined some of the effects to be retained by any statistical model of the turbulent breakup of bubbles at low Weber numbers,

- Resonance phenomenon between the frequency of oscillation of the bubble immersed within the flow and the interaction frequency of the eddies (or strain pulse frequency in the model, T_2).
- Spatial eddy efficiency (concept already suggested by Risso and Fabre), that in our model has been associated to the difference between two strain directions corresponding to successive eddies interacting with the bubble.
- Existence of a minimum effective time of eddy-bubble interaction, T_1, which depends on the Weber number. Moreover, our simulations showed that when T_1 is greater than this minimum value, the breakup is mainly determined by the pulse repetition period, T_2. For example, in terms of our dimensionless formulation this minimum value of T_1 is approximately 0.5 for $We = 1.5$.

However, the limitations of the two-dimensional model proposed here are evident. First, the breakup patterns adopted by the bubble are restricted by the symmetry condition imposed in the formulation. For instance, the lenticular morphology identified by Hinze [2] could never be obtained. A second and important limitation of the present model is that it cannot properly describe the last stages of the breakup process when the neck, of radius r_n, collapses very rapidly, following a law given by $(t_b - t) \propto r_n^2\sqrt{-2\ln r_n}$ or $r_n \propto (t_b - t)^{1/3}$ in the axisymmetric case, at times very short compared with the breakup time [19], t_b.

Acknowledgements

This collaborative research was supported by the Spanish Ministry of Education and European Union under Projects# DPI2002-04550-C07 and DPI2005-08654-C04-01. AR also wants to acknowledge the support of the Ramón y Cajal program.

Appendix A. Linear oscillations of a two-dimensional bubble in a potential straining flow

In this appendix, the oscillatory dynamics of a two-dimensional bubble placed at the origin of a potential straining flow is considered in the limit of low strain rates. The velocity field outside the bubble is given by a velocity potential, ϕ, that satisfies Laplace's equation which in polar coordinates can be written

$$\partial_r(r\,\partial_r\phi) + 1/r\,\partial_\alpha^2\phi = 0 \tag{A.1}$$

being $r = (x^2 + y^2)^{1/2}$ and α the polar angle in a coordinate system such that the angle of the strain pulse $\theta = 0$. The velocity potential, ϕ, must satisfy Eq. (2.4) in the limit $r \to \infty$. In addition, the following boundary conditions

$$-\partial_t f + \partial_r \phi - \frac{1}{(1+f)^2}\partial_\alpha \phi \partial_\alpha f = 0, \text{ and} \tag{A.2}$$

$$p_0(t) - p(r,\alpha,t) = \frac{1}{We}\nabla\cdot\vec{n} = \frac{1}{We}\frac{1+2(\partial_\alpha f/(1+f))^2 - \partial_\alpha^2 f/(1+f)}{(1+f)(1+(\partial_\alpha f/(1+f))^2)^{3/2}}, \tag{A.3}$$

where $p_0(t)$ stands for the pressure inside the bubble, must be fulfilled at the bubble interface given by

$$F(r,\alpha,t) \equiv r - 1 - f(\alpha,t) = 0. \tag{A.4}$$

Notice that outside the bubble, in the liquid phase, the pressure can be related to the velocity potential throughout the Bernouilli equation

$$\partial_t \phi + \frac{1}{2}|\nabla\phi|^2 + p = P(t), \tag{A.5}$$

where $P(t)$ is an arbitrary function of time.

In the limit of low strain rates, $We \ll 1$, the above system of equations, and the boundary conditions, can be linearized by neglecting the quadratic or higher order terms in ϕ and f. Thus Eqs. (A.2), (A.3) and (A.5) simplify to

$$-\partial_t f + \partial_r \phi = 0, \tag{A.6}$$

$$p_0 - p = \frac{1}{We}\big[1 - (\partial_\alpha^2 f + f)\big], \quad \text{and} \tag{A.7}$$

$$\partial_t \phi + p = P \tag{A.8}$$

respectively. The pressure, p, can be eliminated by combining Eqs. (A.7) and (A.8) and, without loss of generality, the arbitrary function of time appearing in the Bernouilli equation can be set to $P(t) = p_0 - 1/We$, to yield

$$\partial_t \phi + \frac{1}{We}(\partial_\alpha^2 f + f) = 0. \tag{A.9}$$

Eq. (A.9) together with Eqs. (A.1) and (A.6), form a system of equations and boundary conditions that determine the two unknown functions ϕ and f. This system of equations will be solved seeking a solution in the form

$$\phi(r,\alpha,t) = M(t)\frac{r^2}{4}\cos 2\alpha + \sum_{n=2}^{\infty} r^{-n}\big[a_n(t)\cos n\alpha + b_n(t)\sin n\alpha\big], \tag{A.10}$$

$$f(\alpha,t) = \sum_{n=2}^{\infty}\big[g_n(t)\cos n\alpha + h_n(t)\sin n\alpha\big]. \tag{A.11}$$

The proposed expansion for ϕ and f is a solution of the problem whenever the set of functions $\{g_n, h_n, a_n, b_n\}$ satisfy the following set of ordinary differential equations

$$-\dot{g}_2 + \frac{M}{2} - 2a_2 = 0, \tag{A.12}$$

$$\frac{\dot{M}}{4} + \dot{a}_2 - \frac{3}{We}g_2 = 0, \tag{A.13}$$

for the second eigenmode $\{g_2, a_2\}$ and

$$-(\dot{g}_n, \dot{h}_n) - n(a_n, b_n) = 0, \tag{A.14}$$

$$(\dot{a}_n, \dot{b}_n) - \frac{1}{We}(n^2-1)(g_n, h_n) = 0 \tag{A.15}$$

for $\{g_n, a_n\}$ with $n > 2$ and $\{h_n, b_n\}$ with $n \geqslant 2$. Notice that Eqs. (A.12) and (A.13) can be combined to yield

$$\ddot{g}_2 + \frac{6}{We}g_2 = \dot{M}. \tag{A.16}$$

The first result is that the motion of the bubble interface, as well as the velocity potential, can be described as a linear combination of the eigenfunctions $\{\cos n\alpha, \sin n\alpha\}$ with coefficients that oscillate with angular frequencies $\omega_n = \sqrt{n(n^2-1)/We}$, with $T_n^{\text{osc}} = 2\pi/\omega_n$. But more importantly, it can also be observed that the time-changing intensity of the straining flow, $M(t)$, is only present in Eqs. (A.12)–(A.13), associated with the second eigenmode $\{g_2, a_2\}$. This result means that, in the limit $We \ll 1$, the outer flow is only able to exchange energy with the $n = 2$ mode of vibration. Therefore, transfer of energy from the outer flow to other eigenmodes, as well as energy transfer between them, is just included in the higher order terms of the governing equations, and can be neglected in a first approximation.

To conclude this appendix, it must pointed out that in a train of successive strain pulses, as the angle of strain $\theta(t)$ changes with time, the outer flow will also transfer energy to the mode $\{b_2, h_2\}$. Nevertheless, notice that there is still not transfer of energy to modes with $n > 2$.

References

[1] A.N. Kolmogorov, On the breakage of drops in a turbulent flow, Dokl. Akad. Nauk SSSR 66 (1949) 825–828.
[2] J.O. Hinze, Fundamentals of the hydrodynamics mechanism of splitting in dispersion processes, AIChE J. 1 (1955) 289–295.
[3] F. Risso, J. Fabre, Oscillations and breakup of a bubble immersed in a turbulent field, J. Fluid Mech. 372 (1998) 323–355.
[4] M. Sevik, S.H. Park, The splitting of drops and bubbles by turbulent fluid flow, Trans. ASME J. Fluid Eng. 3 (1973) 53–60.
[5] J. Rodríguez-Rodríguez, J.M. Gordillo, C. Martínez-Bazán, Break-up time and morphology of drops and bubbles in a high Reynolds number flow, J. Fluid Mech. 548 (2006) 69–86.
[6] C. Martínez-Bazán, J.L. Montañes, J.C. Lasheras, On the breakup of an air bubble injected into a fully developed turbulent flow. Part I: Breakup frequency, J. Fluid. Mech. 401 (1999) 157–182.
[7] I.S. Kang, L.G. Leal, Numerical solution of axisymmetric, unsteady free-boundary problems at finite Reynolds number. I. Finite-difference scheme and its application to the deformation of a bubble in a uniaxial straining flow, Phys. Fluids 30 (1987) 1929–1940.
[8] I.S. Kang, L.G. Leal, Bubble dynamics in time-periodic straining flows, J. Fluid Mech. 218 (1990) 41–69.
[9] A. Revuelta, J. Rodríguez-Rodríguez, C. Martínez-Bazán, Bubble break-up in a straining flow at finite Reynolds number, J. Fluid Mech. 551 (2006) 175–184.
[10] D. Qian, K. Sankaranarayanan, S. Sundaresan, K. Kontomaris, J. B Mc Laughlin, Simulation of bubble dynamics in homogeneous turbulence, Chem. Engrg. Commun. 193 (2006) 1038–1063.
[11] V. Cristini, J. Blawzdziewicz, M. Loewenberg, L.R. Collins, Breakup in stochastic Stokes flows: sub-Kolmogorov drops in isotropic turbulence, J. Fluid Mech. 492 (2003) 231–250.
[12] J.C. Lasheras, C. Eastwood, C. Martínez-Bazán, J.L. Montañes, A review of statistical models for the break-up of an immiscible fluid immersed into a fully developed turbulent flow, Int. J. Multiphase Flow 28 (2002) 247–278.
[13] K. Sarkar, W.R. Schowalter, Deformation of a two-dimensional drop at non-zero Reynolds number in time periodic extensional flows: numerical simulation, J. Fluid Mech. 436 (2001) 177–206.
[14] X. Li, K. Sarkar, Drop dynamics in an oscillating extensional flow at finite Reynolds numbers, Phys. Fluids 17 (2005) 027103.
[15] F.J. Higuera, Axisymmetric inviscid interaction of a bubble and a vortex ring, Phys. Fluids 16 (2004) 1156–1159.
[16] M. Sussman, P. Smereka, Axisymmetric free boundary problems, J. Fluid Mech. 341 (1997) 269–294.
[17] M. Sussman, E. Fatemi, P. Smereka, S. Osher, An improved level-set method for incompressible two-phase flows, Computers and Fluids 27 (1998) 663–680.
[18] T.A. Davis, I.S. Duff, A combined unifrontal/multifrontal method for unsymmetric sparse matrices, ACM Trans. Math. Software 25 (1999) 1–19.
[19] J.M. Gordillo, A. Sevilla, J. Rodríguez-Rodríguez, C. Martínez-Bazán, Axisymmetric bubble pinch-off at high Reynolds numbers, Phys. Rev. Lett. 95 (2005) 194501.